Effect of combined treatment with zoledronic acid and parathyroid hormone on mouse bone callus structure and composition

Michele Casanova[1], Janelle Herelle[1], Marcel Thomas[1], Rowan Softley[1], Aaron Schindeler[2,3], David Little[2,3], Philipp Schneider[1,4], Ralph Müller[1]

Journal of submission:

The Bone Journal, Elsevier

[1] Institute for Biomechanics, ETH Zurich, Zurich, Switzerland

[2] Orthopaedic Research and Biotechnology, The Children's Hospital at Westmead, Westmead, Australia

[3] Discipline of Paediatrics and Child Health, University of Sydney, Camperdown, Australia

[4] Bioengineering Science Research Group, Faculty of Engineering and the Environment, University of Southampton, Southampton, UK

Authors:

Michele Casanova, Institute for Biomechanics, HCP H 22.1, Leopold-Ruzicka-Weg 4, ETH Zurich, 8093 Zurich, Switzerland, tel: +41 44 633 22 43, email: mcasanova@ethz.ch

Janelle Herelle, Institute for Biomechanics, HCP H 22.1, Leopold-Ruzicka-Weg 4, ETH Zurich, 8093 Zurich, Switzerland, tel: +41 44 633 22 43, email: herellej@alum.mit.edu

Marcel Thomas, Institute for Biomechanics, HCP H 22.1, Leopold-Ruzicka-Weg 4, ETH Zurich, 8093 Zurich, Switzerland, tel: +41 44 633 22 43, email: thomamar@ethz.ch

Rowan Softley, Institute for Biomechanics, HCP H 22.1, Leopold-Ruzicka-Weg 4, ETH Zurich, 8093 Zurich, Switzerland, tel: +41 44 633 22 43, email: rsoftley1@gmail.com

Aaron Schindeler, Orthopaedic Research and Biotechnology, The Children's Hospital at Westmead, Westmead, NSW, 2145, Australia tel +61 29 845 14 51, fax +61 29 845 30 78, email: aaron.schindeler@sydney.edu.au

David Little, Orthopaedic Research and Biotechnology, The Children's Hospital at Westmead, Westmead, NSW, 2145, Australia tel +61 29 845 33 52, fax +61 29 845 30 78, email: david.little@health.nsw.gov.au

Switzerland, tel: +41 44 633 72 76, email: rsoftley1@gmail.com

Philipp Schneider, Building 7/Room 4031, Mailpoint M7, Bioengineering Science Research Group, Faculty of Engineering and the Environment, University of Southampton, Southampton. UK, tel +44 23 805 946 40, email: p.schneider@soton.ac.uk

Corresponding author:

Ralph Müller, Institute for Biomechanics, HCP H 23.1, Leopold-Ruzicka-Weg 4, 8093 Zürich, Switzerland, tel: +41 44 632 45 92, fax: +41 44 633 11 24, email: ram@ethz.ch

Number of words:

abstract = 402, manuscript = 5132

Number of figures:

color = 0, black/white = 4

Disclosures:

Prof Little & Dr Schindeler have previously received funding and in-kind support from Amgen, Novartis, Celgene, and N8 Medical for research studies not directly related to this project.

Abstract

In recent years, great interest in combined treatment of parathyroid hormone (PTH) with anti-resorptive therapy has emerged. PTH has been suggested to aid bridging of atrophic fractures and improve strength in closed fracture models. Bisphosphonate treatments typically result in a larger woven bone callus that is slower to remodel. The combination of both drugs has been demonstrated to be effective for the treatment of osteoporotic bone loss in many preclinical studies. However, the effect of combined treatment on fracture repair is still largely unexplored. In this study, we aimed to compare these drugs as single-agent and in combination in a murine closed fracture model. We wanted to assess potential differences in material properties, morphometry and in the development of the lacuno-canalicular network. A total of 40 female, 11-week-old wild type mice underwent a closed fracture on the midshaft of the tibia and were assigned to four groups (n=8-10 per group). Beginning on post-operative day 8, animals received different subcutaneous injections. Group 1 received a single injection of saline solution and Group 2 of zoledronic acid (ZA). Group 3 received daily dosing of PTH. Group 4 received a dual treatment, starting with a single dose of ZA followed by daily injection of PTH. Three weeks after fracture, all animals were euthanized and tibiae were assessed using micro-computed tomography (micro-CT), high-resolution micro-CT (HR micro-CT), Raman spectroscopy, quantitative

histomorphometry, and deconvolution microscopy (DV microscopy). Combined treatment showed a significant increase of 41% in bone volume fraction and a significant decrease of 61% in the standard deviation of the trabecular spacing compared to vehicle, both known to be strong predictors of callus strength. An analysis via HR micro-CT showed similar results on all groups for lacunar numerical density, whereas mean lacuna volume was found to be higher compared to vehicle in treated groups, but only PTH mono-treatment showed a significant increase compared to vehicle (+45%). Raman spectroscopy did not reveal detectable changes in material properties of the bone calluses. Sclerostin staining, tartrate resistant acid phosphatase (TRAP) staining and canalicular analysis with DV microscopy on a subset of samples did not display distinctive difference in any of the treatments.

We therefore consider PTH+ZA treatment beneficial for bone healing. No clear negative effect on bone quality was detected during this study.

Keywords:

Bone healing; bone quality; zoledronic acid; parathyroid hormone; micro-computed tomography; Raman spectroscopy

1. Introduction

Both systemic anabolic and anti-catabolic agents are used clinically to modulate bone turnover, particularly in individuals with osteoporosis or metabolic bone disease. PTH (1-34) is a potent anabolic drug that is commonly used to increase bone formation in osteoporotic patients [1-4]. Bisphosphonates (BPs) are also routinely used to treat osteoporosis and potently suppress bone resorption, leading to a higher bone mass [5, 6]. Zoledronic acid (ZA) is a third generation nitrogen-containing bisphosphonate, and it is one of the most potent BPs in current clinical use [7, 8]. In the past years, we gained expertise in its administration and in the understanding of its effect as anti-catabolic agent in preclinical studies [9-11].

PTH treatment has been suggested as a method for reducing the local osteonecrotic effects that are a rare adverse event associated with BP treatment [12]. PTH may also lead to improvements in bone quality in combination with BP by enabling the repair of microdamage, which if untreated can lead to fracture [13].

Studies reporting on the effect of combined PTH or teriparatide and BPs treatment show conflicting results for preventing bone loss in humans [14-25]. Some studies found PTH treatment to diminish morphological and/or microarchitectural measures when combined with BPs [14, 20, 21, 25]. In other investigations, a significant increase in bone mineral density or an improvement of the microarchitecture was observed [18, 19, 24].

Combined treatment with PTH and BPs during fracture repair is still largely unexplored with a limited number of studies investigating the combination [26-29]. A study of Li *et al.* showed a significant increase of mechanical strength in osteoporotic rat femoral calluses with combined PTH+ZA treatment compared to vehicle and to mono-treatments [26]. However, no study to date has specifically addressed bone quality and material properties of the bone formed under these conditions. We hypothesized that combined treatment with PTH and ZA (PTH+ZA) would increase bone volume and improve bone callus quality with respect to macro-/microarchitecture and material composition by accelerating the healing process.

The study design was to examine the effects of PTH+ZA on the structure and composition of the fracture callus in a mouse tibial fracture model, compared to mono-treatments and no treatment three weeks post-operative (post-op). We therefore wanted to examine the impact of bone modulating drugs on the early stages of callus quality, osteocyte embedding and canalicular formation. We believe that a deeper knowledge on the effects of treatments at different hierarchical levels of the bone healing process will help find a better interpretation of past and future studies focusing on PTH-BP treatments [30]. Eleven-week-old mice which underwent closed tibial fracture were used in this study. Three weeks after inducing the fracture, animals were euthanized. Calluses and contralateral intact tibiae were then extracted for analysis.

Outcome measures included bone standard bone morphometrical measures, such as bone volume fraction (BV/TV) and bone mineral density (BMD) or tissue mineral density (TMD), in both the callus and the contralateral tibiae. To investigate differences in the microstructure of the callus struts, high-resolution micro-computed tomography (HR micro-CT) was adopted. Since in recent years it was suggested that changes in osteocyte lacunar numerical density and size might significantly alter bone stiffness [31], a lacunar analysis was also performed. Possible changes in compositional properties were evaluated with Raman spectroscopy, both in the calluses and in the contralateral tibiae. To gain insight into the underlying cellular expression a limited number of samples were checked for osteocytic expression of the SOST protein and for osteoblastic expression of the tartrate-resistant acid phosphate (TRAP). In addition, we also checked for differences in canalicular density in the latter samples.

By exploring the effects of interventions that reduce and augment remodeling, this study provides a detailed insight into how modulating these fundamental processes affects bone quality during repair.

2. Materials and methods

2.1 Animals, treatments and radiography

Female C57BL/6 mice were purchased from the Animal Resources Center (Perth, WA, Australia) and used at eleven weeks of age. All animals underwent a closed tibial fracture and were assigned to four groups (n=10 per group). Fractures were induced in the midshaft by three point bending with an in-house-made surgical instrument. Groups 1 and 2 received a single subcutaneous (subQ) injection on post-op day 8 of saline solution (VEH) and ZA (0.1 mg/kg), respectively. Group 3 received daily subQ injections of PTH (1-34) (25 µg/kg) starting from post-op day 8. Group 4 received a dual treatment, starting with a subQ injection of ZA (0.1 mg/kg) on post-op day 8 and of daily subQ injections of PTH (25 µg/kg) starting on the same day. Three weeks after fracture, all animals were harvested and their tibiae extracted. All animal experiments were approved by the Westmead Hospital Animal Ethics Committee.

Fracture repair was monitored by radiography (Faxitron X-ray, Tucson, AZ, USA) one week, two weeks and three weeks after fracture. We then assessed union rate for the three time points for each group.

2.2 Micro-CT

Micro-CT analyses were performed according to standard procedures [32, 33]. To assess bone volume fraction and bone mineral density of the calluses, eight to ten samples per group were scanned using a desktop micro-CT system (Skyscan 1174; Aartselaar, Belgium). We excluded two calluses we classified as proximal and the non-unions, since they tend to have a reduced bone volume and could therefore bias our results. An isotropic voxel size of 12 µm, a tube voltage of 50 kVp, a source current of 800 µA and an exposure time of 4.5 s were set. Calluses were scanned to include all new deposited bone (axial dimension of the stack varying between 6.5 and 10.2 mm depending on the callus). A Gaussian filter (sigma=1.2, support=2.0) was applied for noise reduction. We used CT analyzer software (Skyscan, Aartselaar, Belgium) to manually contour the newly formed bone, except for the bone in the intramedullary canal and cortical bone [34]. We then quantified total callus volume (CV), total volume (TV), bone volume (BV), callus BV/TV and BMD according to standard procedures [35].

To assess the effect of the drugs on the intact bone, eight contralateral tibiae per group were also scanned using a HR micro-CT system (µCT 50; Scanco Medical, Brüttisellen, Switzerland). An isotropic voxel size of 2 µm, a tube voltage of 55 kVp, a source current of 72 µA and an exposure time of 10.5 s were set. A stack with a height of approximately 1.1 mm was acquired starting

proximally at 45% of the tibial length. This distance corresponds to the height where the fracture was created in the opposite tibia (fractured bone). After scanning, a Gaussian filter (sigma=0.8, support=1.0) was applied for noise reduction. All cortical bone from the samples was manually contoured and isolated from the scan [36]. We then evaluated with the µCT evaluation program of Image Processing Language (IPL, V6.5-1; Scanco Medical, Brüttisellen, Switzerland). BV/TV, TMD (excluding canals), cortical thickness (Ct.Th) and cortical area (Ct.Ar) were computed.

To assess callus trabecular microarchitecture, seven to eight samples per group were re-scanned using a HR micro-CT system (µCT 50; Scanco Medical, Brüttisellen, Switzerland). An isotropic voxel size of 6 µm, a tube voltage of 55 kVp, a source current to 72 µA, and an exposure time to 7.5 s were set. A Gaussian filter (sigma=0.8, support=1.0) was applied for noise reduction. We then applied a global threshold for all calluses and used IPL to manually contour the newly formed bone. We excluded all cortical bone and the bone formed in the intramedullary canal [34]. Moreover, in order to isolate the callus struts, we used IPL to manually exclude regions where newly formed bone did not present a trabecular structure. For this purpose, regions in which porosity was inferior to the 50% of the local total volume were considered dense woven bone and excluded (isolated trabecular structure; Figure 1, left). BV/TV of the isolated trabecular structure (Tb.BV/TV), Trabecular number

(Tb.N), trabecular thickness (Tb.Th), trabecular separation (Tb.Sp), standard deviation of Tb.Th (Tb.Th.SD), standard deviation of Tb.Sp (Tb.Sp.SD), degree of anisotropy (DA), connectivity density (Conn.D) and the structure model index (SMI) were then computed. Moreover, we computed the polar moment of inertia of the whole callus (cortical bone, dense woven bone and intramedullary bone included) on these high-resolution datasets.

To investigate lacunar numerical density and mean lacuna volumes, six to seven samples per group were scanned again with higher resolution (Figure 1 right). Two stacks with a total height of 180 µm were acquired from the central portion of the callus. An isotropic voxel size of 1.2 µm, a tube voltage of 70 kVp, an intensity of 57 µA and an exposure time of 9 s were selected. Old bone and newly formed bone were manually segmented using customized IPL file scripts. Lacunar numerical density (defined as number of lacunae to bone volume + lacunar porosities) and mean lacuna volumes (defined as total lacunar volume divided by number of lacunae) were inferred from both bone types.

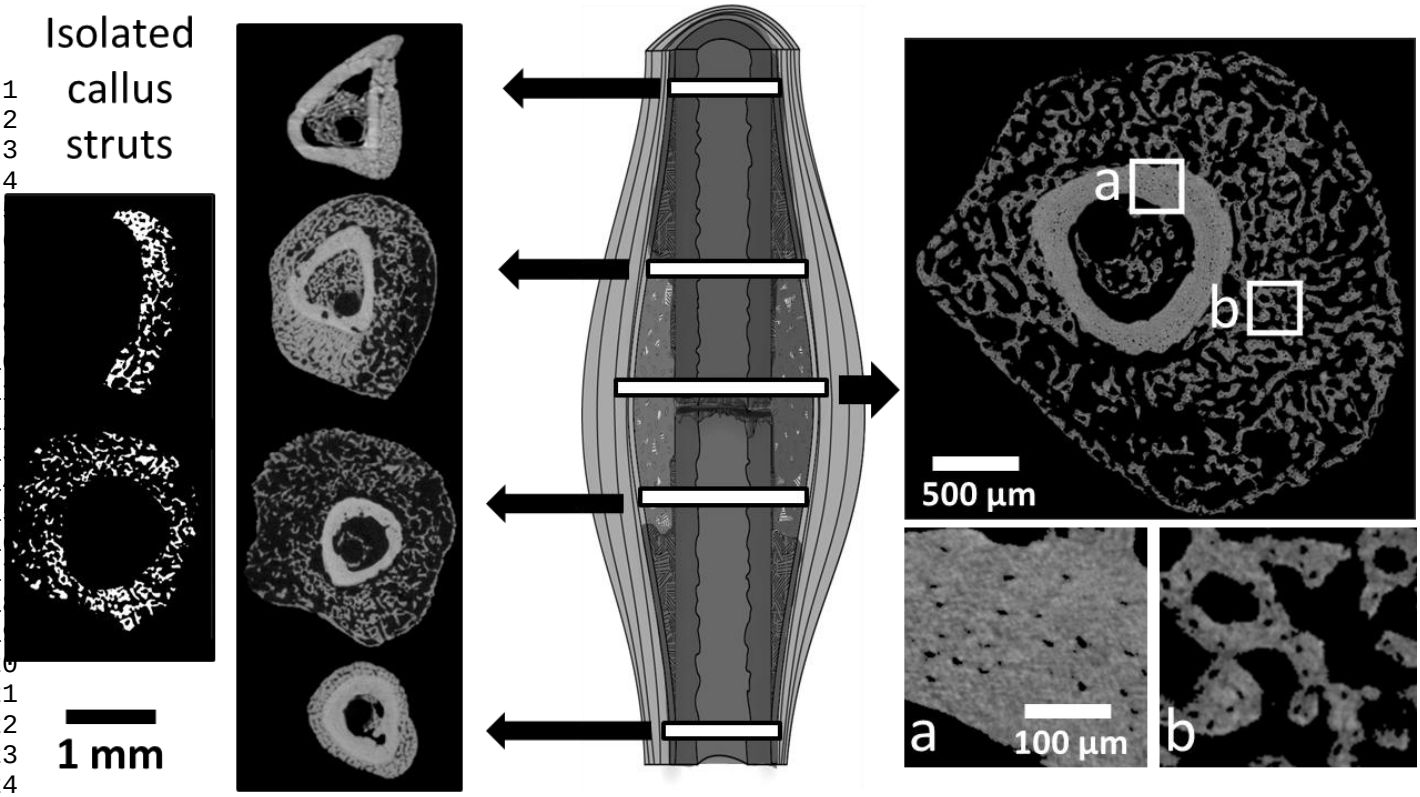

Figure 1 (left) A schematic representation of the isolation of the trabecular region of the callus. The regions with dense woven bone were removed since they are not suited for trabecular analysis. **(right)** High-resolution acquisition for lacunar analysis in the old bone (a) and in the new bone (b).

2.3 Raman spectroscopy

To investigate material composition, six to seven calluses per group and eight contralateral tibiae per group were analyzed with a confocal Raman spectroscope (CRM 200; Witec, Ulm, Germany). The instrument was operated with a green polarized laser at a wavelength of 532 nm, a grating of 900 gr/mm, an objective magnification of 20X and a numerical aperture of 0.75. An

integration time of 20 s, a hardware accumulation of 5 s and a software accumulation of 1 s were applied to every measurement.

All measurements were performed on the periosteal-dorsal site of the tibia. Nine measurements on a 3 x 3 grid (covering an area of 200 µm x 200 µm) were performed on unpolished surface of the central portion of the calluses (outer layer) starting proximally at 45% of the tibial length. Each point was measured under 5 different polarization angles of the laser (-90°, -45°, 0°, 45°, and 90°).

Spectra were analyzed using a custom MATLAB script. For correcting for fluorescence background and computing peak areas, we manually defined a global start point and a global end point for each peak (ν1 phosphate: 925-985 cm^{-1}; carbonate: 1055-1110 cm^{-1}; amide I: 1590-1720 cm^{-1}) and we applied a linear baseline removal between each of these set of two points. Ratios were computed through division of the peak areas. We retrieved mineral-to-matrix ratio [37, 38], carbonate-to-phosphate ratio [37, 39], carbonate-to-amide I ratio [37], crystallinity [40] and degree of collagen orientation [41]. Spectral peaks in Raman spectroscopy are observed to have a sinusoidal behavior with respect to the orientation of the incident polarized laser [41, 42]. Therefore, for each point all ratios obtained from the 5 polarization angles were fitted to a sinusoidal curve with a custom MATLAB script. Mean vertical shifts of the sinusoidal fit of the ratios were used to determine the mean value of the measures. The collagen degree of orientation was computed,

inferring the mean amplitude of the sinusoidal fit normalized by the vertical shift of the ν1 phosphate-to-amide I ratio [41].

2.4 Immunohistochemistry and canalicular expression

To get an insight into osteoblast activity, osteocyte activity and canalicular expression, 3 calluses per treatment group were fixed in 4% phosphate-buffered formalin overnight at 4°C and then cryosectioned. Sections of 5 and 12 µm were obtained from the central portion of the callus cutting the bone longitudinally (in the sagittal plane).

Five micrometer sections were stained for tartrate-resistant acid phosphatase (TRAP), which was performed using a fluorescent ELFR97 Phosphatase Substrate (Molecular Probes, Eugene, OR, USA). Osteoclast surface (Oc.S/BS) was then assessed on a section per sample, by evaluating the posterior half of the newly formed bone of the section. Sclerostin staining was also performed on 5 µm sections, which were incubated in anti-sclerostin primary antibody (R&D Systems, Minneapolis, MN, USA). Secondary antibody detection was accomplished using the DAB substrate kit SK-4100 (Vector Labs, Burlingame, CA, USA). We then manually counted sclerostin positive osteocyte and total number of osteocyte on the newly formed bone of the posterior half of the section.

Twelve micrometer sections were used to investigate canalicular expression. Sections were stained in 1% fluorescein isothiocyanate

(FITC) overnight and analyzed using a deconvolution microscope (Deltavision, Issaquah, WA, USA). The osteocyte processes were isolated in the cortical bone and the newly formed bone from regions in the middle of the cortex of the samples (old bone) and from the central portion of the callus (newly formed bone). In two regions, datasets of 60 stacks with a thickness of 0.2 µm and a magnification of 60X were acquired. The images were then post-processed using ImageJ (U. S. National Institutes of Health, Bethesda, MD, USA) and the osteocytes at a depth greater than 2 µm were considered for determining the region of interest (ROI). As canaliculi are emanating radially from the lacunae, the ROI was placed on sections of the stack located 1 µm above the upper part of the osteocyte lacuna, so that the canaliculi were aligned as perpendicular as possible to the ROI for their quantification (Figure 2). The ROI had to be sufficiently extended to cover the projection of the lacuna (Figure 2A-B) and it was then translated to the section used for the canalicular detection. The images were subsequently processed using edge enhancement and they were thresholded to facilitate canalicular counting (Figure 2C). The number of processes that trespass the ROI was divided by the ROI area in μm^2. In each of the twelve samples, the cell processes of 8 to 12 osteocytes were analyzed.

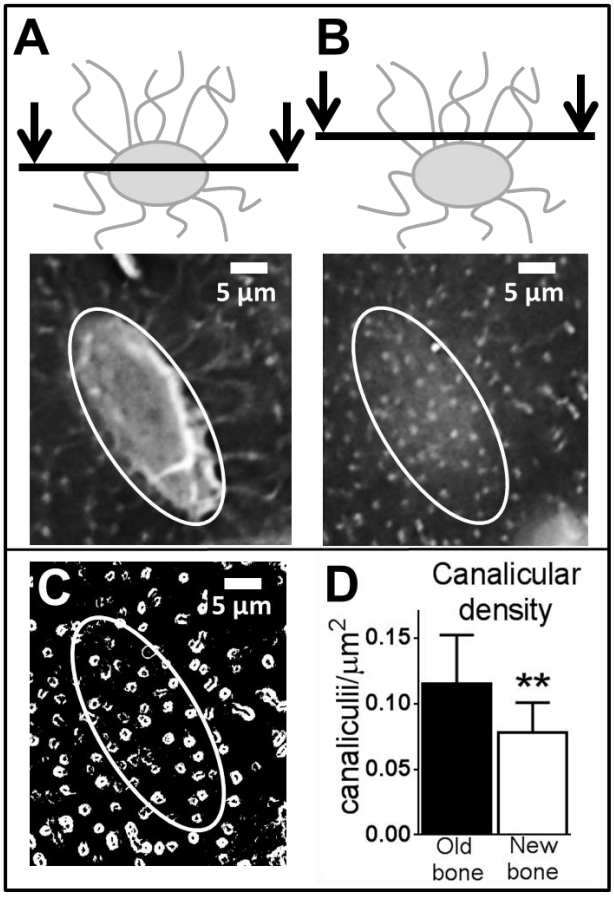

Figure 2 Representation of the method to quantify number of osteocyte processes. **(A)** The osteocyte lacuna is included in the ROI **(B)** A confocal plane of about 1 µm above the lacuna is selected. **(C)** The images were then processed for counting. **(D)** Bar plot of the canalicular density of the osteocyte in the old bone (n=90) and newly formed bone (n=87). Treatment groups are pooled. Asterisks represent significance ($p<0.01$).

2.5 Statistical analysis

All statistical analyses were performed using SPSS Statistics (version 20; IBM, Armonk, NY, USA). Mean and standard deviation (SD) were given for all the results. One-way ANOVA with Bonferroni post-hoc test was used for the analysis of the morphometric results of the contralateral tibiae. For all the other

comparisons between treatment groups, a Kruskal-Wallis test was adopted. To investigate which groups differ, pairwise comparisons with adjusted significance were performed according to the procedure proposed by Dunn [43]. A Wilcoxon signed-rank test with data pooled across groups was used for detecting differences between contralateral and fractured tibiae in Raman spectroscopy-derived measures. Additionally, a Wilcoxon signed-rank test with data pooled across groups was performed for detecting differences in lacunar measures and canalicular number density between old bone and newly formed bone in the callus. For all analyses, $p \leq 0.05$ was considered to indicate statistical significance.

3. Results

3.1 Animals, treatments & radiography

Radiographs showed that at one week post-op no group had bridged calluses. At two weeks post-op, four calluses of vehicle, four of ZA, five of PTH and two of PTH+ZA appeared to not have completely bridged. At three weeks post-op, all but two calluses had bridged: a ZA sample experienced an intramedullary pin failure and did not heal properly, whereas a VEH sample broke during pin removal. These samples were excluded from the study. Moreover, two fractures were classified proximal.

3.2 Micro-CT

Results from quantitative micro-CT macro-/microarchitecture, BMD, TMD and lacunar measures are summarized in Table 1 and Figure 3. Significantly higher callus BV/TV and BMD were found in all treated calluses compared to VEH (VEH vs. mono-treatments: $p < 0.05$, VEH vs. PTH+ZA: $p < 0.001$). Figure 3A depicts bar plots for callus BV/TV and BMD (numerical values in the supplementary material; Table S.1). PTH+ZA treatment showed the highest value for both parameters. The contralateral tibiae only presented a significant difference in BV/TV between ZA and PTH treatment ($p < 0.05$).

Representative longitudinal cross-sections for each treatment group are depicted in Figure 4. PTH+ZA treatment showed significantly higher values in Trab.BV/TV ($p < 0.05$), Tb.N ($p < 0.01$) and Conn.D ($p < 0.01$) compared to VEH. It also showed significant lower values in Tb.Sp ($p < 0.01$), Tb.Sp.SD ($p < 0.01$), Tb.Th.SD ($p < 0.01$), and DA ($p < 0.01$) compared to VEH. Bar plots for Tb.N and Tb.Sp.SD are presented in Figure 3B (numerical values in Table S.1). Lacunar numerical density (N.Lc/BV) did not show any significant difference between groups. However, we found lacunar numerical density in newly formed bone of the groups to be significantly higher than old bone ($p < 0.05$). PTH treated group mean lacuna volume was significantly larger than VEH in old bone ($p < 0.05$). Also in newly formed bone, PTH treatment showed

significantly larger mean lacuna volume ($p < 0.01$). Bar plots for lacunar numerical density and mean lacuna volumes for the different treatment in old and newly formed bone are presented in Figure 3C (numerical values in Table S.1).

Table 1 Quantitative micro-computed tomography macro-/microarchitecture and bone mineral density of the newly formed bone (new bone) and old bone. Trabecular microarchitectural measures of new bone exclude the original cortices and the dense woven bone in the calluses. Old bone refers to bone of the contralateral tibia for microarchitectural measures. CV: total callus volume, TV: total volume; BV: bone volume; BV/TV: bone fraction; TMD: tissue mineral density Ct.Th: cortical thickness; Ct.Ar: cortical area; Tb.BV/TV: bone volume fraction of the trabecular structure; Tb.Th: trabecular thickness; Tb.Sp: trabecular separation; Tb.Th.SD: standard deviation of Tb.Th; DA: degree of anisotropy; Conn.D: connectivity density; SMI: structure model index; J: polar moment of inertia; VEH: saline treated group; ZA: zoledronic acid treated group; PTH: parathyroid hormone (1-34) treated group. PTH+ZA: combined PTH and ZA treated group; SD: standard deviation.

	VEH (SD)	ZA (SD)	PTH (SD)	PTH + ZA (SD)
Macroscopic measures				
New bone	*N=8*	*N=9*	*N=9*	*N=10*
CV (mm^3)	15.6 (7.9)	18.5 (4.6)	17.4 (4.8)	17.0 (5.3)
TV (mm^3)	14.8 (8.2)	18.7 (4.7)	17.6 (4.9)	16.8 (5.7)
BV (mm^3)	7.97 (3.4)	14.2 (3.0)*	13.5 (3.7)	13.7 (4.3)
Old bone (contralateral tibia)	*N=8*	*N=8*	*N=8*	*N=8*
BV/TV (%)	58.0 (1.7)	57.4 (0.7)	61.4 (4.1) #	60 (3.2)
TMD (HA mg/cm^3)	1.11 (0.01)	1.11 (0.02)	1.11 (0.01)	1.11 (0.01)
Ct.Th (mm)	0.206 (0.006)	0.205 (0.009)	0.218 (0.009)	0.217 (0.011)
Ct.Ar (mm^2)	0.545 (0.020)	0.531 (0.030)	0.566 (0.028)	0.568 (0.029)
Microarchitectural measures				
New bone	*N=7*	*N=7*	*N=8*	*N=8*
Tb.BV/TV (%)	21.7 (8.9)	26.1 (6.4)	23.1 (3.8)	33.1 (5.8)*,+
Tb.Th (mm)	0.0456 (0.085)	0.0372 (0.003)	0.0354 (0.003)**	0.0363 (0.002)*
Tb.Sp (mm)	0.135 (0.047)	0.093 (0.19)	0.094 (0.02)	0.067 (0.010)**
Tb.Th.SD (mm)	0.019 (0.008)	0.013 (0.002)	0.014 (0.005)	0.011 (0.001)**
DA (-)	1.25 (0.09)	1.08 (0.04)*	1.11 (0.03)	1.07 (0.03)**
Conn.D ($1/mm^3$)	1024 (431)	1968 (484)	1878 (596)	2375 (377)***
SMI (-)	1.18 (1.18)	1.30 (0.52)	1.77 (0.20)	1.00 (0.60)+
J (mm^4)	0.78 (0.30)	1.67 (0.36)*	1.65 (0.56)*	1.32 (0.40)

*: $p < 0.05$ when compared to VEH; **: $p < 0.01$ when compared to VEH group, ***: $p < 0.001$ when compared to VEH group; #: $p < 0.05$ when compared to ZA group; +: $p < 0.05$ when compared to PTH group.

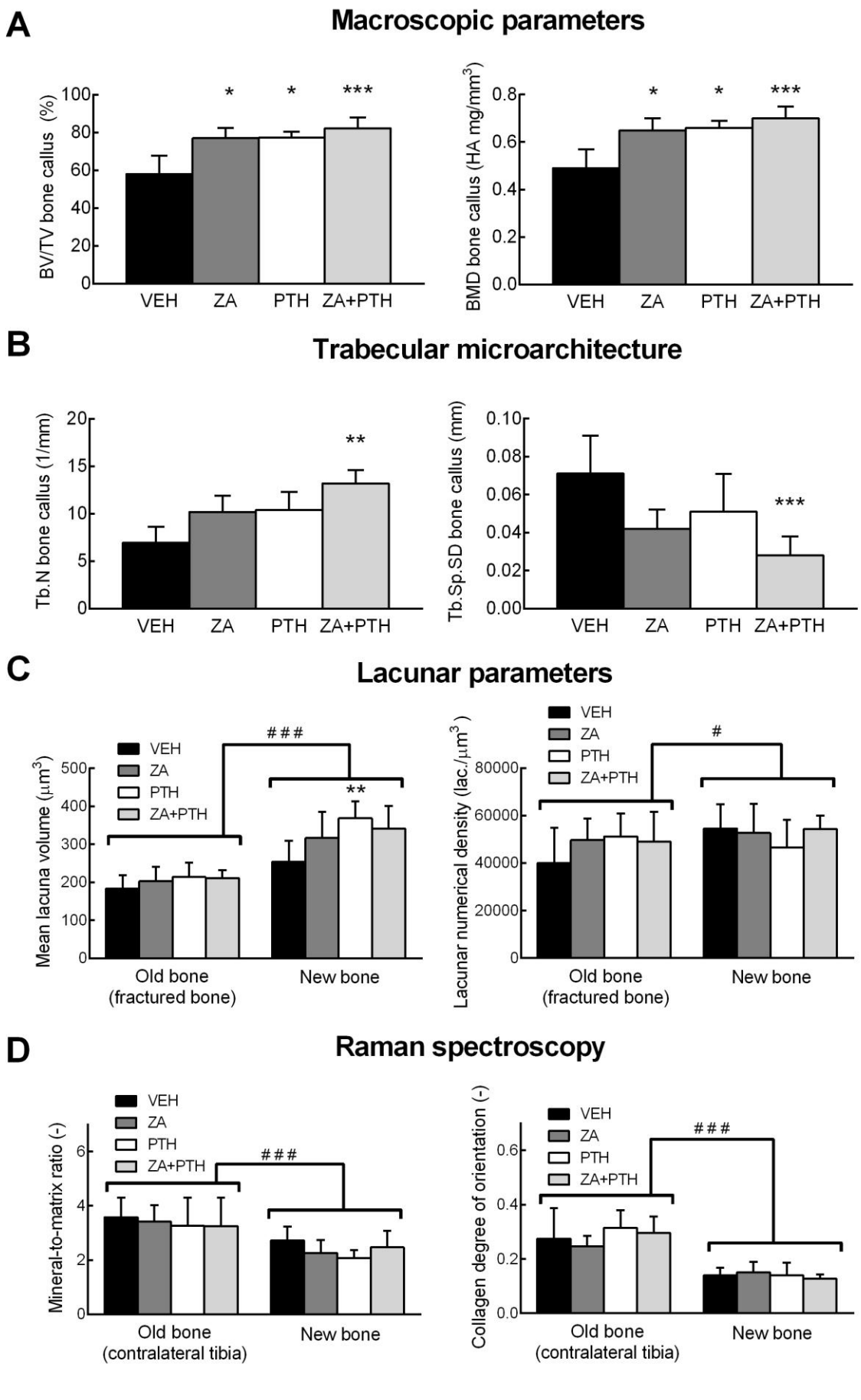
A
Macroscopic parameters
BV/TV bone callus (%)
BMD bone callus (HA mg/mm3)
VEH
ZA
PTH
ZA+PTH
B
Trabecular microarchitecture
Tb.N bone callus (1/mm)
Tb.Sp.SD bone callus (mm)
C
Lacunar parameters
Mean lacuna volume (μm3)
Lacunar numerical density (lac./μm3)
Old bone (fractured bone)
New bone
D
Raman spectroscopy
Mineral-to-matrix ratio (-)
Collagen degree of orientation (-)
Old bone (contralateral tibia)
New bone

Figure 3 Summary of selected results obtained in this study. **(A)** Macroscopic measures: bone fraction (BV/TV) and bone mineral density (BMD) of the callus; **(B)** Trabecular microarchitecture: trabecular number (Tb.N) and standard deviation of the trabecular separation (Tb.Sp.SD). Trabecular microarchitectural measures of new bone exclude the original cortices and the dense woven bone in the calluses **(C)** Lacunar parameters: mean lacuna volumes and lacunar numerical density of the cortical and newly formed bone in the callus; **(D)** Raman spectroscopy: mineral-to-matrix ratio and collagen degree of orientation of the contralateral tibia and of the newly formed bone. Asterisks (*) represent significant difference between treatments and hash character (#) represent significance difference between cortical or old and new bone (pooled data). VEH: saline treated group; ZA: zoledronic acid treated group; PTH: parathyroid hormone (1-34) treated group. PTH+ZA: combined parathyroid hormone (1-34) and zoledronic acid treated group. Error bars represents ± 1 standard deviation.

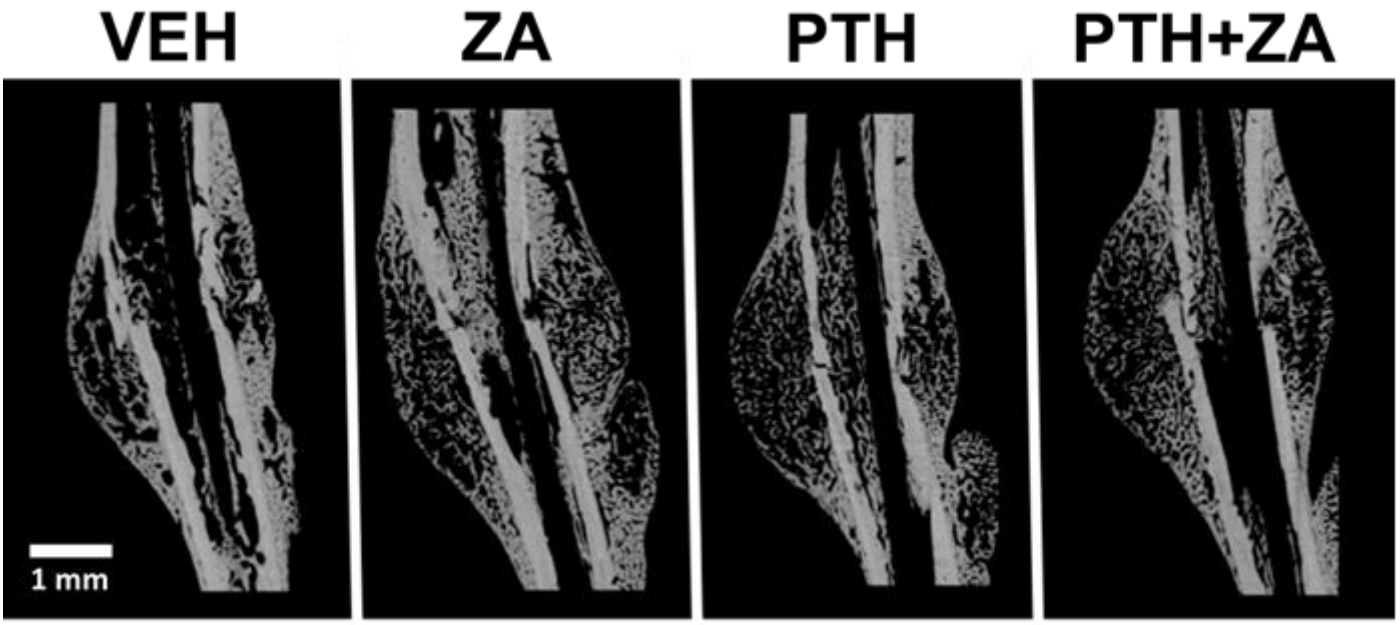

Figure 4 Representative longitudinal cross-sections of the murine calluses for each treatment group. VEH: saline treated group; ZA: zoledronic acid treated group; PTH: parathyroid hormone (1-34) treated group. PTH+ZA: combined parathyroid hormone (1-34) and ZA treated group.

3.3 Raman spectroscopy

Table 2 and Figure 3D summarize the results for the Raman spectroscopy experiments. Raman spectroscopy did not show significant changes between treatments in the newly formed bone. The mean coefficient of determination R^2 for the sinusoidal fit of the 5 acquisitions was 0.72 for the calluses and 0.95 for the contralateral tibiae. Higher values for R^2 in the contralateral tibiae are due to a stronger collagen orientation which results in a large variation of the amplitude of the sinusoidal fit with consequent increase of the squared residuals with respect to the average value.

Contralateral bone presented significantly higher values compared to newly formed bone for all measures ($p < 0.01$). We noticed a

significant difference in carbonate-to-phosphate ratio between PTH treated groups and VEH in the contralateral groups ($p < 0.05$). Bar plots for mineral-to-matrix ratio and the degree of collagen orientation are depicted in Figure 3D (numerical values in Table S.2).

Table 2 Overview of the Raman spectroscopy measures for each group both of the newly formed bone (new bone) and of the contralateral tibia. C:P: carbonate-to-phosphate ratio, C:AmI: carbonate-to-amide I ratio; VEH: saline treated group; ZA: zoledronic acid treated group; PTH: parathyroid hormone (1-34) treated group. PTH+ZA: combined PTH and ZA treated group; SD: standard deviation.

	VEH (SD)	ZA (SD)	PTH (SD)	PTH+ZA (SD)
Raman quality measures				
New bone	*N=6*	*N=6*	*N=7*	*N=7*
C:P (-)	0.089 (0.006)	0.087 (0.008)	0.084 (0.015)	0.089 (0.014)
C:AmI (-)	0.241 (0.055)	0.195 (0.042)	0.176 (0.044)	0.215 (0.048)
Crystallinity (1/cm)	0.0456 (0.0006)	0.0446 (0.0006)	0.0447 (0.0017)	0.0445 (0.0008)
Old bone (contralateral tibia)	*N=8*	*N=8*	*N=8*	*N=8*
C:P (-)	0.104 (0.006)	0.098 (0.004)	0.089 (0.009)*	0.090 (0.007)*
C:AmI (-)	0.364 (0.058)	0.331 (0.062)	0.291 (0.111)	0.285 (0.089)
Crystallinity (1/cm)	0.0461 (0.0002)	0.0453 (0.0005)	0.0456 (0.0006)	0.0455 (0.0009)

*: $p < 0.05$ when compared to VEH group.

3.4 Immunohistochemistry & canalicular expression

Results of immunohistochemistry and canalicular expression are summarized in Table 3. No distinctly different expression was found in the combined- nor the mono-treatments. However, we observed a

significantly higher canalicular expression in cortical bone osteocytes compared to newly formed bone osteocytes ($p < 0.01$, Figure 2D).

Table 3 Osteoclast surface (Oc.S/BS), sclerostin positive osteocytes to total number of osteocytes (Pos. Oc/all Oc), and canalicular number density (N.Cn/Ar) in old bone and newly formed bone (new bone) for the four treatments. VEH: saline treated group; ZA: zoledronic acid treated group; PTH: parathyroid hormone (1-34) treated group. PTH+ZA: ZA and PTH treated group; SD: standard deviation.

	VEH (SD)	ZA (SD)	PTH (SD)	PTH+ZA (SD)
Cellular expression	*N=3*	*N=3*	*N=3*	*N=3*
Oc.S/BS (-)	0.17 (0.07)	0.13 (0.04)	0.13 (0.04)	0.21 (0.07)
Pos. Oc/all Oc (%)	41 (15)	42 (9)	42 (10)	25 (9)
Canalicular number density	*N=3*	*N=3*	*N=3*	*N=3*
N.Cn/Ar old bone ($1/\mu m^2$)	0.22 (0.07)	0.17 (0.05)	0.17 (0.06)	0.18 (0.05)
N.Cn/Ar new bone ($1/\mu m^2$)	0.12 (0.03)	0.15 (0.04)	0.12 (0.03)	0.11 (0.02)

4. Discussion

This study used a range of outcome modalities to analyze the effects of administering PTH and ZA mono- and combination treatments on the fracture callus. Both anabolic and anti-catabolic treatments led to fundamental changes in structure and trabecular microarchitecture, but did not significantly change material composition compared to VEH at three weeks. Whether changes in mineralization could have occurred over longer time periods has not been investigated in this study. Treatments might have shown larger effects on factors such as

total callus volume in later phases of fracture repair, but this was not the aim of this investigation. Weekly radiography showed that two weeks post-op, combined treatment had the lowest number of not completely bridged calluses (two versus four calluses in VEH). This can be seen as a positive outcome for the combined treatment, although numbers are too low to draw any definitive conclusions. As observed in prior studies [24, 26, 29], combined treatment resulted in higher values of bone mass and BMD. The combination of PTH+ZA was also found to improve trabecular microarchitecture compared to mono-treatments. According to a recent study by Mehta *et al.* [44], the most important trabecular microarchitectural predictors of callus strength are Tb.N, Tb.Sp.SD and Tb.Th. In their study, these measures explained up to the 57% of the variability of callus strength [44]. PTH+ZA treatment had the highest value for Tb.N and the lowest value for Tb.Sp.SD. Tb.Th decreased with all treatments and in PTH and PTH+ZA treated groups this difference was significant. The VEH group created a structure with fewer but thicker trabeculae. Due to the smaller number of struts, great strains are experienced and remodeling probably stimulates the struts to increase their size. On the other hand, treated calluses have a completely different trabecular microarchitectural structure, with a larger amount of thinner struts. This is visible in Figure 4, where VEH longitudinal cross-section distinguishes itself from treatments' cross-sections by its thicker and sparser struts. The difference in structure may point to the fact that the treatment groups can distribute force more equally in

their network. This particular response of the trabecular structure is consistent with studies investigating trabecular microarchitecture of newly formed bone after administration of PTH or BPs [45-47], which tends to decrease Tb.Th. The effect of PTH or BPs on the microstructure of bone found in other studies is presented in Table S.3. Although struts thinner than 12 µm can potentially be missing in our datasets for the analysis of the trabecular microarchitecture due to partial volume effect [35], such thin struts were not observable in our histological sections and are not likely to play a relevant role in the mechanical behavior of the callus [48]. Polar moment of inertia was significantly higher in ZA and PTH groups compared to VEH. The larger callus structure formed by ZA and PTH treated fractures was largely responsible for increasing this result since given the size of these calluses a larger fraction of bone is located farther away from the centroid. Nevertheless, different studies did not find a strong correlation of polar moment of inertia with callus strength [34, 44, 48]. It seems that the assumption required by the computation of the polar moment of inertia of tissue shear modulus being constant throughout the callus does not match the actual mechanical behaviour [34]

Recently, correlations between bone porosity and fracture risk were suggested [49, 50]. Changes in lacunar numerical density and size were suggested to induce changes in bone stiffness [31], since lacunae are believed to act as stress concentrators where microcracks are observed [51]. Therefore, an increase in lacunar numerical density or size could possibly lead to higher chances of fracture,

especially in the callus where lacunar porosity can account for a large fraction of the thin struts.

The mean lacuna volume was significantly larger in the PTH treated group compared to VEH in newly formed bone. A phenomenon caused by PTH known as osteocytic osteolysis [52-54] was already observed in cortical bone [55, 56] and could possibly explain the results. To our knowledge, this is the first time this is observed in newly formed bone during fracture healing. An increase in lacunar size was also experienced in the PTH+ZA treatment group although apparently, osteocytic osteolysis seems to be slightly reduced possibly due to the co-injection of ZA.

Lacunar numerical density was found to be higher in newly formed bone compared to old bone. This difference was already observed in previous studies on histological sections [57, 58]. We hypothesize that the increase is originally due to a higher number of osteoblasts in healing bone as compared to cortical bone. Lacunar numerical density provides a history of the development of the mineral tissue, since osteoblasts entomb themselves in the mineral matrix and create the lacunae. Since the bone surface area of newly formed bone is larger due to the trabecular structure, the number of osteoblasts per bone volume will be higher. Moreover, due to the need to rapidly increase bone volume, more osteoblast will be recruited. These cells will lay bone and embed themselves in the callus struts and there will be consequently more osteocytes per bone volume. Conversely,

no significant differences in lacunar numerical density were detected between treatment groups neither in newly formed bone nor in old bone. Since an increased number of lacunae might be correlated with fracture risk, we regard this result favorable for PTH+ZA treatment.

Raman spectroscopy has already been applied to investigate changes in newly formed bone due to drug treatments [59], showing relatively large variances within fracture calluses. In our study, we could not observe any detectable change in material composition in newly formed bone between the different treatments. Significant differences were detected between calluses and intact tibiae, which partly validates the sensitivity of the measurements. We also observed a significant decrease in carbonate-to-phosphate ratio in the contralateral tibia of PTH treated groups, where carbonate-to-phosphate ratio is related to the age of the bone with low values indicating higher bone turnover [60]. The contralateral results are in accordance with the anabolic effect of PTH which leads to new bone formation in the periosteal region [61].

Collagen orientation in the callus did not differ between groups, neither in cortical bone nor in newly formed bone. We were expecting samples treated with ZA to show less oriented collagen fibers due to the decrease in callus remodeling knowingly caused by BPs. Nevertheless, a recent study on the effects of ZA on newly formed bone showed changes in collagen structure only with high-dosages (600 μg/kg), whereas dosages similar to ours were not found

to affect collagen structure [62]. A significantly lower degree of collagen orientation was however observed between calluses and intact bone, which is in accordance with previous findings [63, 64].

The analysis of SOST+ osteocytes and TRAP+ osteoclasts did not reveal any significant differences. All groups showed a similar value of Oc.S/BS (TRAP) and sclerostin positive osteocytes to total number of osteocytes (SOST). We did not observe a lower value of Oc.S/BS for the groups that received ZA.

We found a significant difference between the number of canaliculi in cortical bone and newly formed bone (Figure 2D). Newly formed bone expressed less canaliculi per area than newly formed bone, which was already observed in previous studies using other methodologies [65]. Nevertheless, we did not observe any differences in the canalicular expression between treatments.

Study limitations

Some limitations of this study warrant discussion. Raman spectroscopy was performed after the samples had been scanned using micro-CT at least three times. This long exposure to room temperature and possibly also the exposure to X-rays could have altered the material properties of the samples. An increase in white noise in the Raman spectra compared to fresh-frozen bone samples was observed. We suggest, for future studies involving Raman spectroscopy, to plan the experiments in a fashion which limits the

exposure time of the samples to room temperature. Moreover, the long acquisition time required for lacunar resolution limited us to the analysis of relatively small volumes. Operating with larger regions of interest may identify differences in lacunar numerical densities, e.g. between the central region of the callus and the dense woven bone found at the extremities of the callus (which may differ between treatments). Mechanical testing would have also been of interest. Although this study did not examine whole bone mechanics, prior studies have already addressed this point [26-29].

5. Conclusions

We hypothesized PTH+ZA could improve bone callus quality with respect to macro-/microarchitecture and/or material composition. PTH+ZA treatment showed an improvement in both bone mass measures and trabecular microarchitecture. At a lacunar level, we observed that treatments did not significantly alter lacunar numerical density in the fracture callus. However, an increased mean lacuna volume was found in PTH mono-treatment and in the combined treatment. This volume enlargement may be due to increased osteocytic osteolysis caused by PTH and opens new interesting questions on this process, since to our knowledge it is the first time that this phenomenon is observed in regenerating bone. Further investigation is required to ascertain if this increase in mean lacuna volume could possibly weaken the structure. Raman spectroscopic

measures did not differ between groups in the callus, which we interpret as a sign that treatments did not negatively alter bone composition. We also did not find any distinctive difference in osteoblastic activity, osteocytic activity and canalicular expression between treatments.

We therefore consider PTH+ZA treatment beneficial for fracture repair. The increase in mean lacuna volume with PTH treatment alone could affect local tissue stiffness, but whether this is a negative effect on bone quality is not known.

Acknowledgements

The authors would like to thank Bastien Chatton, Mille Kolind, Nicole Yu and Andreas Trüssel for their technical assistance.

Conflict of Interest

The authors declare no conflict of interest.

References

[1] Qin L, Raggatt LJ, Partridge NC. Parathyroid hormone: a double-edged sword for bone metabolism. Trends Endocrinol Metab 2004;15: 60-5.

[2] Goltzman D. Studies on the mechanisms of the skeletal anabolic action of endogenous and exogenous parathyroid hormone. Arch Biochem Biophys 2008;473: 218-24.

[3] Datta NS, Abou-Samra AB. PTH and PTHrP signaling in osteoblasts. Cell Signal 2009;21: 1245-54.

[4] Sibai T, Morgan EF, Einhorn TA. Anabolic agents and bone quality. Clinical Orthopaedics and Related Research® 2011;469: 2215-2224.

[5] Wilkinson JM, Little DG. Bisphosphonates in orthopedic applications. Bone 2011;49: 95-102.

[6] Rodan GA, Fleisch HA. Bisphosphonates: mechanisms of action. J Clin Invest 1996;97: 2692-6.

[7] Reid IR, Brown JP, Burckhardt P, Horowitz Z, Richardson P, Trechsel U, Widmer A, Devogelaer JP, Kaufman JM, Jaeger P, Body JJ, Brandi ML, Broell J, Di Micco R, Genazzani AR, Felsenberg D, Happ J, Hooper MJ, Ittner J, Leb G, Mallmin H, Murray T, Ortolani S, Rubinacci A, Saaf M, Samsioe G, Verbruggen L, Meunier PJ. Intravenous zoledronic acid in postmenopausal women with low bone mineral density. N Engl J Med 2002;346: 653-61.

[8] Black DM, Delmas PD, Eastell R, Reid IR, Boonen S, Cauley JA, Cosman F, Lakatos P, Leung PC, Man Z, Mautalen C, Mesenbrink P, Hu H, Caminis J, Tong K, Rosario-Jansen T, Krasnow J, Hue TF, Sellmeyer D, Eriksen EF, Cummings SR, Trial HPF. Once-yearly zoledronic acid for treatment of postmenopausal osteoporosis. N Engl J Med 2007;356: 1809-22.

[9] McDonald MM, Dulai S, Godfrey C, Amanat N, Sztynda T, Little DG. Bolus or weekly zoledronic acid administration does not delay endochondral fracture repair but weekly dosing enhances delays in hard callus remodeling. Bone 2008;43: 653-662.

[10] Schindeler A, Little DG. Osteoclasts but not osteoblasts are affected by a calcified surface treated with zoledronic acid in vitro. Biochemical and biophysical research communications 2005;338: 710-716.

[11] Bobyn J, Rasch A, Mikulec K, Schindeler A, Little D. Combination Therapy with Bone Morphogenetic Protein 2 (BMP-2) and Zoledronic Acid (ZA) Improves Posterolateral Spinal Fusion in a Mouse Model of Neurofibromatosis Type 1. In: Journal of Bone Mineral Research; 2013.

[12] Kwon YD, Lee DW, Choi BJ, Lee JW, Kim DY. Short-term teriparatide therapy as an adjunctive modality for bisphosphonate-related osteonecrosis of the jaws. Osteoporosis International 2012;23: 2721-2725.

[13] Ettinger B, Burr D, Ritchie R. Proposed pathogenesis for atypical femoral fractures: lessons from materials research. Bone 2013;55: 495-500.

[14] Black DM, Greenspan SL, Ensrud KE, Palermo L, McGowan JA, Lang TF, Garnero P, Bouxsein ML, Bilezikian JP, Rosen CJ, Pa THSI. The effects of parathyroid hormone and alendronate alone or in combination in postmenopausal osteoporosis. N Engl J Med 2003;349: 1207-15.

[15] Cosman F, Nieves J, Zion M, Woelfert L, Luckey M, Lindsay R. Daily and cyclic parathyroid hormone in women receiving alendronate. N Engl J Med 2005;353: 566-75.

[16] Jakob F, Oertel H, Langdahl B, Ljunggren O, Barrett A, Karras D, Walsh JB, Fahrleitner-Pammer A, Rajzbaum G, Barker C, Lems WF, Marin F. Effects of teriparatide in postmenopausal women with osteoporosis pre-treated with bisphosphonates: 36-month results from the European Forsteo Observational Study. Eur J Endocrinol 2012;166: 87-97.

[17] Cosman F, Keaveny TM, Kopperdahl D, Wermers RA, Wan X, Krohn KD, Krege JH. Hip and spine strength effects of adding versus switching to teriparatide in postmenopausal women with osteoporosis treated with prior alendronate or raloxifene. J Bone Miner Res 2013;28: 1328-36.

[18] Cosman F, Eriksen EF, Recknor C, Miller PD, Guanabens N, Kasperk C, Papanastasiou P, Readie A, Rao H, Gasser JA, Bucci-Rechtweg C, Boonen S. Effects of intravenous zoledronic acid plus subcutaneous teriparatide [rhPTH(1-34)] in postmenopausal osteoporosis. J Bone Miner Res 2011;26: 503-11.

[19] Muschitz C, Kocijan R, Fahrleitner-Pammer A, Lung S, Resch H. Antiresorptives overlapping ongoing teriparatide treatment result in additional increases in bone mineral density. J Bone Miner Res 2013;28: 196-205.

[20] Finkelstein JS, Hayes A, Hunzelman JL, Wyland JJ, Lee H, Neer RM. The effects of parathyroid hormone, alendronate, or both in men with osteoporosis. N Engl J Med 2003;349: 1216-26.

[21] Finkelstein JS, Wyland JJ, Lee H, Neer RM. Effects of teriparatide, alendronate, or both in women with postmenopausal osteoporosis. J Clin Endocrinol Metab 2010;95: 1838-45.

[22] Tsai JN, Uihlein AV, Lee H, Kumbhani R, Siwila-Sackman E, McKay EA, Burnett-Bowie SA, Neer RM, Leder BZ. Teriparatide and denosumab, alone or combined, in women with postmenopausal osteoporosis: the DATA study randomised trial. Lancet 2013;382: 50-6.

[23] Schafer AL, Burghardt AJ, Sellmeyer DE, Palermo L, Shoback DM, Majumdar S, Black DM. Postmenopausal women treated with combination parathyroid hormone (1-84) and ibandronate demonstrate different microstructural changes at the radius vs. tibia: the PTH and Ibandronate Combination Study (PICS). Osteoporos Int 2013;24: 2591-601.

[24] Altman AR, Tseng WJ, de Bakker CM, Huh BK, Chandra A, Qin L, Liu XS. A closer look at the immediate trabecula response to combined parathyroid hormone and alendronate treatment. Bone 2014;61: 149-57.
[25] Wu X, Pang L, Lei W, Lu W, Li J, Li Z, Frassica FJ, Chen X, Wan M, Cao X. Inhibition of Sca-1-positive skeletal stem cell recruitment by alendronate blunts the anabolic effects of parathyroid hormone on bone remodeling. Cell Stem Cell 2010;7: 571-80.
[26] Li YF, Zhou CC, Li JH, Luo E, Zhu SS, Feng G, Hu J. The effects of combined human parathyroid hormone (1-34) and zoledronic acid treatment on fracture healing in osteoporotic rats. Osteoporos Int 2012;23: 1463-74.
[27] Aspenberg P, Wermelin K, Tengwall P, Fahlgren A. Additive effects of PTH and bisphosphonates on the bone healing response to metaphyseal implants in rats. Acta Orthop 2008;79: 111-5.
[28] Arrington SA, Fisher ER, Willick GE, Mann KA, Allen MJ. Anabolic and antiresorptive drugs improve trabecular microarchitecture and reduce fracture risk following radiation therapy. Calcif Tissue Int 2010;87: 263-72.
[29] Hashimoto T, Shigetomi M, Ohno T, Matsunaga T, Muramatsu K, Tanaka H, Sugiyama T, Taguchi T. Sequential treatment with intermittent low-dose human parathyroid hormone (1-34) and bisphosphonate enhances large-size skeletal reconstruction by vascularized bone transplantation. Calcif Tissue Int 2007;81: 232-9.
[30] Casanova M, Schindeler A, Little D, Muller R, Schneider P. Quantitative phenotyping of bone fracture repair: a review. Bonekey Rep 2014;3: 550.
[31] Yeni YN, Vashishth D, Fyhrie DP. Estimation of bone matrix apparent stiffness variation caused by osteocyte lacunar size and density. J Biomech Eng 2001;123: 10-7.
[32] Bouxsein ML, Boyd SK, Christiansen BA, Guldberg RE, Jepsen KJ, Muller R. Guidelines for assessment of bone microstructure in rodents using micro-computed tomography. J Bone Miner Res 2010;25: 1468-86.
[33] Morgan EF, De Giacomo A, Gerstenfeld LC. Overview of skeletal repair (fracture healing and its assessment). Skeletal Development and Repair: Methods and Protocols 2014: 13-31.
[34] Morgan EF, Mason ZD, Chien KB, Pfeiffer AJ, Barnes GL, Einhorn TA, Gerstenfeld LC. Micro-computed tomography assessment of fracture healing: relationships among callus structure, composition, and mechanical function. Bone 2009;44: 335-44.
[35] Bouxsein ML, Boyd SK, Christiansen BA, Guldberg RE, Jepsen KJ, Müller R. Guidelines for assessment of bone microstructure in rodents using micro–computed tomography. Journal of bone and mineral research 2010;25: 1468-1486.
[36] Kohler T, Beyeler M, Webster D, Muller R. Compartmental bone morphometry in the mouse femur: reproducibility and resolution dependence of microtomographic measurements. Calcif Tissue Int 2005;77: 281-90.

[37] Morris MD, Mandair GS. Raman assessment of bone quality. Clin Orthop Relat Res 2011;469: 2160-9.
[38] McCreadie BR, Morris MD, Chen TC, Sudhaker Rao D, Finney WF, Widjaja E, Goldstein SA. Bone tissue compositional differences in women with and without osteoporotic fracture. Bone 2006;39: 1190-5.
[39] Penel G, Leroy G, Rey C, Bres E. MicroRaman spectral study of the PO4 and CO3 vibrational modes in synthetic and biological apatites. Calcif Tissue Int 1998;63: 475-81.
[40] Timlin JA, Carden A, Morris MD. Chemical microstructure of cortical bone probed by Raman transects. Appl Spectrosc 1999;53: 1429-1435.
[41] Makowski AJ, Patil CA, Mahadevan-Jansen A, Nyman JS. Polarization control of Raman spectroscopy optimizes the assessment of bone tissue. J Biomed Opt 2013;18: 55005.
[42] Gamsjaeger S, Masic A, Roschger P, Kazanci M, Dunlop J, Klaushofer K, Paschalis E, Fratzl P. Cortical bone composition and orientation as a function of animal and tissue age in mice by Raman spectroscopy. Bone 2010;47: 392-399.
[43] Dunn OJ. Multiple Comparisons Using Rank Sums. Technometrics 1964;6: 241-252.
[44] Mehta M, Heyland M, Toben D, Duda GN. Microstructure and homogeneity of distribution of mineralised struts determine callus strength. Eur Cell Mater 2013;25: 366-79; discussion 378-9.
[45] Aleksyniene R, Thomsen JS, Eckardt H, Bundgaard KG, Lind M, Hvid I. Three-dimensional microstructural properties of regenerated mineralizing tissue after PTH (1-34) treatment in a rabbit tibial lengthening model. J Musculoskelet Neuronal Interact 2009;9: 268-77.
[46] Takahashi M, Yukata K, Matsui Y, Abbaspour A, Takata S, Yasui N. Bisphosphonate modulates morphological and mechanical properties in distraction osteogenesis through inhibition of bone resorption. Bone 2006;39: 573-81.
[47] Seebach C, Skripitz R, Andreassen T, Aspenberg P. Intermittent parathyroid hormone (1-34) enhances mechanical strength and density of new bone after distraction osteogenesis in rats. J Orthop Res 2004;22: 472-8.
[48] Shefelbine SJ, Simon U, Claes L, Gold A, Gabet Y, Bab I, Muller R, Augat P. Prediction of fracture callus mechanical properties using micro-CT images and voxel-based finite element analysis. Bone 2005;36: 480-8.
[49] Voide R, Schneider P, Stauber M, van Lenthe GH, Stampanoni M, Muller R. The importance of murine cortical bone microstructure for microcrack initiation and propagation. Bone 2011;49: 1186-93.
[50] Carriero A, Doube M, Vogt M, Busse B, Zustin J, Levchuk A, Schneider P, Muller R, Shefelbine SJ. Altered lacunar and vascular porosity in osteogenesis imperfecta mouse bone as revealed by synchrotron tomography contributes to bone fragility. Bone 2014;61: 116-124.

[51] Reilly GC. Observations of microdamage around osteocyte lacunae in bone. J Biomech 2000;33: 1131-4.
[52] Belanger LF. Osteocytic osteolysis. Calcif Tissue Res 1969;4: 1-12.
[53] Teti A, Zallone A. Do osteocytes contribute to bone mineral homeostasis? Osteocytic osteolysis revisited. Bone 2009;44: 11-16.
[54] Wysolmerski JJ. Osteocytic osteolysis: time for a second look? Bonekey Rep 2012;1: 229.
[55] Tommasini SM, Trinward A, Acerbo AS, De Carlo F, Miller LM, Judex S. Changes in intracortical microporosities induced by pharmaceutical treatment of osteoporosis as detected by high resolution micro-CT. Bone 2012;50: 596-604.
[56] Tazawa K, Hoshi K, Kawamoto S, Tanaka M, Ejiri S, Ozawa H. Osteocytic osteolysis observed in rats to which parathyroid hormone was continuously administered. J Bone Miner Metab 2004;22: 524-529.
[57] Parfitt AM. The physiologic and clinical significance of bone histomorphometric data. Bone histomorphometry: techniques and interpretation 1983: 143-223.
[58] Hernandez CJ, Majeska RJ, Schaffler MB. Osteocyte density in woven bone. Bone 2004;35: 1095-9.
[59] Meganck JA, Begun DL, McElderry JD, Swick A, Kozloff KM, Goldstein SA, Morris MD, Marini JC, Caird MS. Fracture healing with alendronate treatment in the Brtl/+ mouse model of osteogenesis imperfecta. Bone 2013;56: 204-12.
[60] Goodyear SR, Gibson IR, Skakle JM, Wells RP, Aspden RM. A comparison of cortical and trabecular bone from C57 Black 6 mice using Raman spectroscopy. Bone 2009;44: 899-907.
[61] Jilka RL, O'Brien CA, Ali AA, Roberson PK, Weinstein RS, Manolagas SC. Intermittent PTH stimulates periosteal bone formation by actions on post-mitotic preosteoblasts. Bone 2009;44: 275-86.
[62] Olejnik C, Falgayrac G, During A, Cortet B, Penel G. Doses effects of zoledronic acid on mineral apatite and collagen quality of newly-formed bone in the rat's calvaria defect. Bone 2016;89: 32-39.
[63] Wen HB, Cui FZ, Feng QL, Li HD, Zhu XD. Microstructural investigation of the early external callus after diaphyseal fractures of human long bone. J Struct Biol 1995;114: 115-22.
[64] Cui FZ, Zhang Y, Wen HB, Zhu XD. Microstructural evolution in external callus of human long bone. Mat Sci Eng C-Bio S 2000;11: 27-33.
[65] Kusuzaki K, Kageyama N, Shinjo H, Takeshita H, Murata H, Hashiguchi S, Ashihara T, Hirasawa Y. Development of bone canaliculi during bone repair. Bone 2000;27: 655-659.